Switching Dynamics of Ag-Based Filamentary Volatile Resistive Switching Devices—Part II: Mechanism and Modeling

Wei Wang, *Member, IEEE*, Erika Covi, *Senior Member, IEEE*, Yu-Hsuan Lin, Elia Ambrosi, Alessandro Milozzi, Caterina Sbandati, Matteo Farronato, *Graduate Student Member, IEEE*, and Daniele Ielmini, *Fellow, IEEE*

***Abstract*— Understanding the switching mechanism of the volatile resistive switching random access memory (RRAM) device is important to harness its characteristics and further enhance its performance. Accurate modeling of its dynamic behavior is also of deep value for its applications both as selector and as short-term memory synapse for future neuromorphic applications operating in temporal domain. In this work, we investigate the switching and retention (relaxation) processes of the Ag-based metallic filamentary volatile resistive switching devices. We find that the switching process can be modeled by the ionic drift under electric field, while the retention process can be modeled by the ionic diffusion along the filament surface driven by the gradient of surface atomic concentration. Through further theoretical analysis, we also find that the ionic drift and ionic diffusion can be unified within the general Einstein relation. To confirm this relation, we collect ionic mobility and diffusivity data from the literature using the switching and retention model. Finally, we show that the read voltage dependent retention time can be explained by the competition between the ionic drift and diffusion flux.**

***Index Terms*— Einstein relation, ionic drift, surface diffusion, volatile memory.**

I. Introduction

VOLATILE resistive switching random access memory (RRAM) devices based on silver (Ag) or copper (Cu) filaments are recently extensively reported with high ON/OFF ratio [1], [2] and steep switching slope [3]. The high ON/OFF ratio originates from the high conductivity of the formed metallic filaments at ON-state and good insulating performance of the switching layer after the filaments dissolution at OFF-state. The high ON/OFF ratio is suitable for selector application in a crossbar array [4], [5]. However, this application is hindered by the relatively long retention/relaxation time of the volatile behavior, i.e., the spontaneous transition from ON-state to OFF-state. Although materials and structure engineering can be used to reduce the retention time to few microseconds [6], in most cases milliseconds or larger retention times are reported, which is similar to the timescales of short-term memory effects in biological neural systems [7]. This leads to emerging applications of using the volatile RRAM device as short-term synaptic or neural device in neuromorphic computation working in temporal domain [8]. For instance, Wang *et al.* [7] utilized this short-term memory effect to naturally emulate spike timing dependent plasticity in a combined synapse consisting of a volatile resistive device based on Ag filament and a nonvolatile resistive device. Zhang *et al.* [9] utilized the volatile-switching dynamics of Ag filamentary device to construct a compact and efficient artificial neuron to integrate input spikes and deliver fires without auxiliary circuits.

The massive implementation of both the conventional and emerging applications calls for deep understanding of the physical mechanisms behind the volatile behavior and accurate modeling of the switching dynamics of this kind of devices. The out-diffusion of filamentary atoms to surrounding dielectric layer for filament dissolution [10], [11] cannot fully account for general transmission electron microscopy (TEM) observations which suggests that the filamentary atoms tend to cluster together [3], [6], [12]. A recently proposed Gibbs–Thomson model for the filamentary atoms nucleation and retraction to electrodes provides a reasonable physical explanation [13], while lacking the accurate prediction ability since the simulated dynamic behavior can only be provided as a function of time in an arbitrary unit [1], [13], [14].

In this work, based on the Ag filamentary volatile RRAM device and its extensive characteristics reported in the

Manuscript received February 12, 2021; revised May 6, 2021; accepted July 1, 2021. Date of publication July 26, 2021; date of current version August 23, 2021. This work was supported in part by Semiconductor Research Corporation under Grant 2018-IN-2814, in part by the European Union's Horizon 2020 Research and Innovation Programme under Grant 824164, in part by the Ministero dell'Istruzione dell'Università e della Ricerca under Grant 2016/R164TYLBZP. Device fabrication was carried out in Polifab, the micro- and nanofabrication facility of the Politecnico di Milano. The review of this article was arranged by Editor P. Narayanan. *(Corresponding author: Daniele Ielmini.)*

Wei Wang, Erika Covi, Elia Ambrosi, Alessandro Milozzi, Caterina Sbandati, Matteo Farronato, and Daniele Ielmini are with the Dipartimento di Elettronica, Informazione e Bioingegneria, Politecnico di Milano, 20133 Milan, Italy (e-mail: daniele.ielmini@polimi.it).

Yu-Hsuan Lin is with the Department of Electronics Engineering, Institute of Electronics, National Chiao Tung University, Hsinchu 30010, Taiwan.

Color versions of one or more figures in this article are available at https://doi.org/10.1109/TED.2021.3095033.

Digital Object Identifier 10.1109/TED.2021.3095033

This work is licensed under a Creative Commons Attribution 4.0 License. For more information, see https://creativecommons.org/licenses/by/4.0/

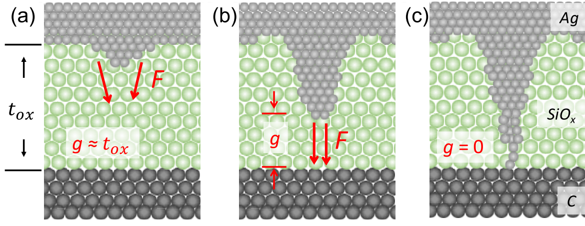

Fig. 1. Schematic of the switching-ON process. (a) Gap approximates oxide thickness before switching. (b) Gap decreasing during the switching-ON process. (c) Switching-ON process ends when a filament connecting top and bottom electrodes is formed.

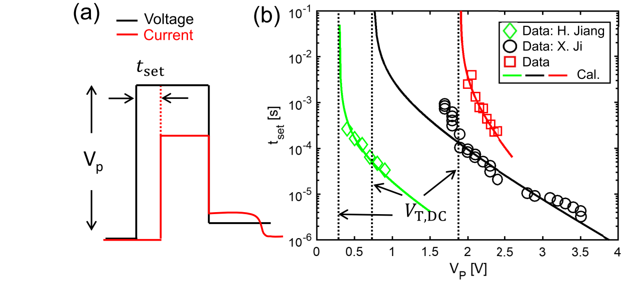

Fig. 2. (a) Schematic of the device switching-ON parameters for rectangular pulse. (b) Experimental data [15] and model calculation of the pulse amplitude dependent switching time, along with data from other literature reports [13], [21].

companion paper [15], we focus on the mechanism investigation and numerical modeling of this device. A preliminary report is presented in IEEE International Electron Device Meeting (IEDM 2019) [16]. Here, we provide an extensive report with fully detailed theoretical study and model derivation. Additional to the IEDM abstract, more data were collected from literature and compared with the model. An extensive discussion was made to state the limitation of the current model and the model's connection with other theories about metallic filamentary RRAM devices.

II. Switching Model

A. Field Driven Filament Growth Model

The high ON/OFF ratio of Ag- or Cu-based volatile memory device indicates that the ON-state has a continuous filament connecting the top and bottom electrodes [Fig. 1(c)], while the OFF-state has a relatively large filament gap (Fig. 1(a), here we assume that the filament gap approximates the oxide layer thickness). The schematic of filament growth during the switching process can be illustrated as in Fig. 1(a)–(c). The switching process might also involve the oxidation of the active electrode materials, i.e., Ag atoms to Ag cations in the top electrode, transportation of the cations across the oxide layer, and reduction of the ionized metal elements in the bottom electrode. This will induce the reversed cone shape of the formed filament in the ON-state [17], different from that shown in Fig. 1(c). Following similar filament shapes observed in TEM [7], [18], and supported by argumentations in the following sections, we assume the filament shape illustrated in Fig. 1(c).

In any case, the filament growth rate is controlled by the electric field F, which is increasing with the decreasing of the filament gap during the growth of the filament as shown in Fig. 1(b). In the oxidation–reduction scenario, the switching-ON speed of the device is also limited by the cation transport velocity in the oxide layer, which should also be electric field controlled [20]. The filament growth velocity is linearly proportional to the velocity of the ions. Since the filament and its tip would be assumed to consist of a small number of atoms, the linear prefactor would be small ($<$10). Despite this approximation, this model can allow the extraction of an approximate value of the mobility to compare with other properties, such as the diffusivity, instead of obtaining the precise value. Thus, the rate equation for the filament gap g is given by

$$dg/dt = -\mu_F F \qquad (1)$$

where t is the time, $\mu_F = \mu_0\, e^{\alpha q(V-V_{\mathrm{T,DC}})/kT}$ is the field controlled mobility of cation ions, μ_0 is the ion mobility at infinitesimal electrical field, α is a constant for barrier lowering of ion transport, q is the ionic charge, V is the voltage applied to the device, $V_{\mathrm{T,DC}}$ is the threshold voltage measured in dc characteristics, k is Boltzmann's constant, and T is the temperature. The electric field is calculated as $F = (V - V_{\mathrm{T,DC}})/g$ since the device would not switch when the voltage is smaller than a minimal value, i.e., the dc threshold voltage. Note that our model primarily aims at extracting the field-independent mobility μ_0, since this is the low-field mobility that should be compared to the diffusivity within the framework of the Nernst–Einstein relation. The exponential part in the equation should be considered as the field-induced barrier lowering that is responsible for the field-acceleration of the set transition.

Instead of electric field, we use the voltage in the exponent of the field controlled mobility. This approximation is to simplify the derivation for the following integration of the rate equation to derive the switching time and to avoid unreasonably high mobility when the gap is approaching zero. We also note that the dc threshold voltage, $V_{\mathrm{T,DC}}$, was considered as a fitting parameter in our model. From our experimental results [15, Fig. 2], we find that the dc threshold voltage is constant and independent of the oxide layer thickness. The forming voltage is linearly proportional to the oxide layer thickness; however, the linear projection to zero thickness is not zero but very close to the subsequent dc threshold voltage. The result is consistent with the previous report on copper-based filamentary RRAM devices [19]. The experimental observations indicate that: 1) a constant electrical field is needed for the forming operation of the devices; 2) the extrapolation of the threshold voltage V_{set} for zero thickness is a nonzero minimal voltage; and 3) this minimal voltage might share the same physical origin with the dc threshold voltage. However, the physical meanings of these findings need to be further explored.

B. Amplitude Dependent Switching Time

For rectangular pulse in the ac measurement [Fig. 2(a)], we find that the switching time, i.e., the set time t_{set}, strongly

depends on the pulse amplitude V_P (Fig. 2(b), red squares). In (1), we can replace the voltage V with the pulse amplitude V_P, obtaining an equation for the differential increase of the filament gap in time, given by

$$dt = \frac{1}{\mu_0(V_P - V_{T,DC})} e^{-\alpha q(V_P - V_{T,DC})/kT} g dg. \quad (2)$$

Integration of (2) over the filament growth process provides the relation between switching time t_{set} and pulse amplitude V_P. In fact, integrating the left-hand side of (2) from time 0 to time t_{set} will result in the switching time t_{set}, while, correspondingly, integrating the right-hand side of (2) for the gap from t_{ox} to 0 [Fig. 1(a)–(c)] will leads to

$$t_{set} = \frac{t_{ox}^2}{2\mu_0} \frac{1}{V_P - V_{T,DC}} e^{-\alpha q(V_P - V_{T,DC})/kT}. \quad (3)$$

Here, only μ_0 and α are unknown variables. Fig. 2(b) shows the experimental data [15] and simulation results from (3) with the parameter value $\mu_0 = 2.5 \times 10^{-10}$ cm^{2}V^{-1}s^{-1} and $\alpha = 0.09$. A similar dataset is also collected from literature [13], [21] and shown in Fig. 2(b) along with the corresponding simulations by (3) with the fitting parameters being $\mu_0 = 3.46 \times 10^{-9}$ cm^{2}V^{-1}s^{-1}, $\alpha = 0.05$ (black line, $t_{ox} = 30$ nm [21]) and $\mu_0 = 10^{-8}$ cm^{2}V^{-1}s^{-1}, $\alpha = 0.05$ (green line, $t_{ox} = 10$ nm [13]), respectively. We always used room temperature for the calculation, which is a good approximation given the high thermal conductivity of the silver filament.

Note that the data in Fig. 2(b) might encourage the idea of exponential decrease of switching time at increasing pulse amplitude. However, this could not be true in the low pulse amplitude region, since extrapolation of an exponential dependence would intersect with the y-axis, meaning that the device can spontaneously switch even at zero bias. For a real threshold switching device, there must be an asymptotic line for the switching time, as indicated by the dashed lines in Fig. 2(b). Our model correlates the position of the asymptotic line with the dc threshold voltage of the device [Fig. 2(b) and (3)].

There are three parameters controlling the voltage dependent switching time in (3). Each of these three parameters have specific impact on the characteristics in Fig. 2: 1) an asymptotic line controlled by the dc threshold voltage, $V_{T,DC}$; 2) the slope in the exponential regime far from the asymptotic line, corresponding to the parameter α; and 3) magnitude of t_{set} taken at a reference voltage corresponding to the mobility μ_0 at infinitesimal electrical field.

C. Ramp-Rate Dependent Threshold Voltage

By applying a half-triangular pulse with maximum voltage V_m and pulsewidth t_p, the device would experience an increasing voltage bias during the switching process [Fig. 3(a)] with the voltage ramp rate denoted by

$$dV/dt = V_m/t_p. \quad (4)$$

Substituting (4) to (2) and rearranging the equation such that only one variable (g or V) can be seen in each side, we obtain

$$g dg = -\frac{\mu_0 \, t_p}{V_m} e^{\alpha q(V - V_{T,DC})/kT} (V - V_{T,DC}) dV. \quad (5)$$

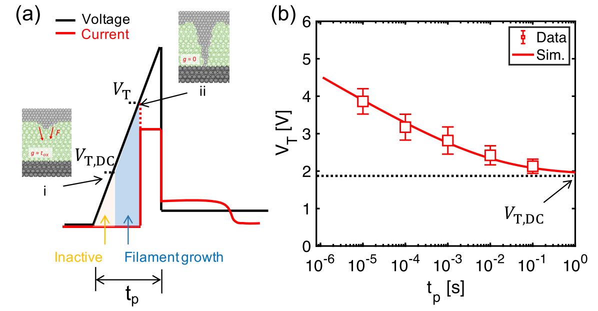

Fig. 3. (a) Schematic of the device switching-ON parameters for half-triangular pulses with various pulsewidth. The filament growth happens after the voltage crosses over $V_{T,DC}$ and ends at threshold voltage V_T. (b) Experimental data in error bars and model calculation of the pulsewidth dependent threshold voltage.

The switching ON process corresponds to the gap from t_{ox} to 0 on the left-hand side of (5) and corresponds to the voltage from to $V_{T,DC}$ to V_T on the right-hand side as illustrated in Fig. 3(a). By integrating both sides of the (5), we get

$$t_p = \frac{t_{ox}^2}{2\mu_0} \frac{V_m}{} \left(\frac{\alpha q}{kT}\right)^2 \frac{1}{exp\left(\frac{\alpha q(V_T - V_{T,DC})}{kT}\right)\left(\frac{\alpha q(V_T - V_{T,DC})}{kT} - 1\right) + 1} \quad (6)$$

where only μ_0 and α are unknown variables.

Fig. 3(b) shows the data from the companion paper [15] and calculation results by (6) with the parameter value of μ_0 and α as in Fig. 2(b), indicating a good agreement between the data and model. The dc threshold voltage is also shown in the figure as the asymptotic line for both data and model.

There are several models dealing with the switching-ON process of filamentary RRAM devices [22]–[28]. However, these models are individual models only considering the switching ON process without considering the spontaneous switching OFF of the filamentary RRAM devices, or they do not link to switching model with the retention model in a unified physical scenario.

III. Retention Model

A. Ionic Surface Diffusion

By molecular dynamic simulations, we have confirmed that a continuous nanoscale Ag filament can spontaneously break without any external forces (Fig. 4 and [29]). During the simulation, we find that only the atoms at the surface of the filament are randomly migrating, while the atoms in bulk remain fixed in their crystalline positions [Fig. 4(a) and (b)]. With the evolution of the filament shape, the inner bulk atoms can be exposed to surface and begin to migrate. The total free energy of the system is also relaxing as the filament shape evolves [Fig. 4(c)]. An energy relaxation higher than 60 eV was evidenced by the molecular dynamics simulation for a filament composed by several thousand atoms. Since there are no external forces applied, the origin of the filament shape evolution is attributed to the surface energy minimization or surface tension effect [29]. The filament evolution model based on surface tension shares the same physical origin

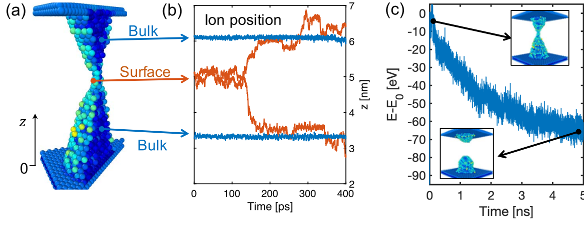

Fig. 4. Molecular dynamics simulations of the relaxation of a nanoscale Ag filament. (a) Sectional view of the simulated nanoscale Ag filament between two fixed planes of silver atoms; the color indicates the kinetic energy of single atom (brighter color, higher energy). (b) Traces of individual atoms: surface atoms diffuse, bulk atoms remain fixed. (c) Total energy relaxation due to the filament relaxation (insets: corresponding filament states).

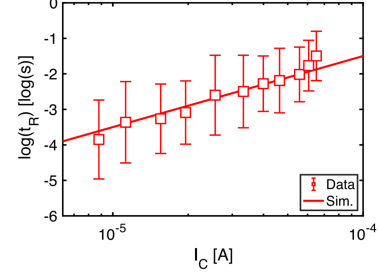

Fig. 5. Experimental and calculated retention time as a function of compliance current.

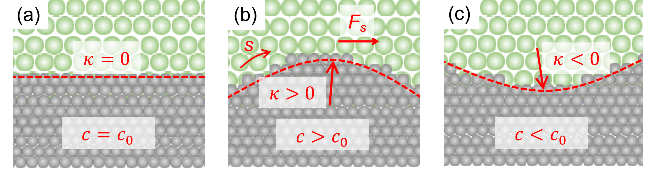

Fig. 6. Schematic of the surface ionic concentration concept used in the surface diffusion model. (a) Flat surface. (b) Surface with positive curvature. (c) Surface with negative curvature.

of Rayleigh instability which has been utilized to analyze the self-dissolution of nanoscale metallic filament in volatile RRAMs [30]. The Rayleigh instability assumes a liquid-like behavior of the metallic filament. However, due to the solid nature of the filament, it is most accurate to assume that only the atoms at the surface of the filament are moving, which then results in the filament shape evolution and disruption.

The retention of the Ag-based volatile device after the pulse can be inferred from the current tails after the pulse in Figs. 2(a) and 3(a) which reveal the spontaneous evolution from an initial filament shape to a disconnected-filament state [Fig. 4(c)] [31]. This surface self-diffusion mechanism has been further confirmed by the existence of ovulation effect starting from ultrathin filament at dc measurement for ultrasmall compliance current as shown in [15, Fig. 3(c)].

B. Size Dependent Retention Time

Through extensive simulations, we find that the device retention time, t_{R}, is strongly depends on the size. An initially large filament (characterized by its diameter in the bottleneck ϕ_0) will result in a relatively long retention time, following Herring's scaling law [29], [31], [32]:

$$t_{\mathrm{R}} = \lambda \phi_0^4 \tag{7}$$

where $\lambda = (3\pi kT)/(16\ D_{\mathrm{S}}\gamma\delta^4)$ is the scaling factor, D_{S} is the surface diffusivity, γ is the surface energy, and δ is the Ag atom dimension.

The filament size in the ON-state can be controlled by the compliance current I_{C} provided by the series transistor in our measurement during the pulse [15]. Assuming a cylinder shape of the filament in the ON-state and a critical voltage V_{c} across the RRAM device at the end of the set transition [33], we can write the compliance current as a function of the filament diameter as

$$I_{\mathrm{C}} = V_{\mathrm{c}}\sigma_0 \frac{\pi\phi_0^2}{4t_{\mathrm{ox}}} \tag{8}$$

where σ_0 is the Ag conductivity. Combining (7) and (8), we can obtain

$$t_{\mathrm{R}} = \beta I_{\mathrm{C}}^2 \tag{9}$$

where $\beta = (3kT/(\pi D_{\mathrm{S}}\gamma\delta^4))(t_{\mathrm{ox}}/V_{\mathrm{c}}\sigma_0)^2$ is a constant.

Fig. 5 shows the retention time as a function of compliance current in log–log scale. The model line is given by (9) with the parameter $\beta = 3.16 \times 10^6\ \mathrm{A}^{-2}\mathrm{s}$ and is a straight line with slope of 2 in the log–log plot, in good agreement with the experimental data.

IV. Ionic Drift and Diffusion

For a consistent ionic drift–diffusion theory, firstly, we note that, similar to the ionic diffusion, the ionic drift should also mainly happen along the filament surface. The reasons for this argument are: 1) continuous metallic filaments are always observed during the switching from *in situ* TEM [7], [34], [35]; 2) the atoms within the metallic filament are in crystalline states as observed in TEM [35] and based on our molecular dynamics simulation, hence hard to be moved; and 3) the electric field within the metallic filament is virtually zero. Also, to quantitatively describe the surface drift and diffusion flux, we need to define the surface atomic/ionic concentration. The surface concentration can be quantitatively described with the help of surface curvature κ and surface energy γ [36] according to

$$c = c_0 e^{\frac{\kappa\gamma\delta^3}{kT}} \tag{10}$$

where c_0 is the ionic concentration at flat metallic surface [Fig. 6(a)]. From (10), metallic surface of positive curvature [Fig. 6(b)] have higher metallic surface concentration than that of negative curvature [Fig. 6(c)]. Thus, the surface ions can spontaneously flow from positive-curvature points [e.g., bottleneck point in Fig. 4(a)] to negative-curvature points [e.g., junction points between the filament and electrode planar in Fig. 4(a)] to minimize the total surface area and energy, thus giving rise to the ionic diffusion flux. Following Fick's first law, the diffusion flow can be obtained by multiplying the ionic diffusivity D_{S} with the negative gradient of the ionic

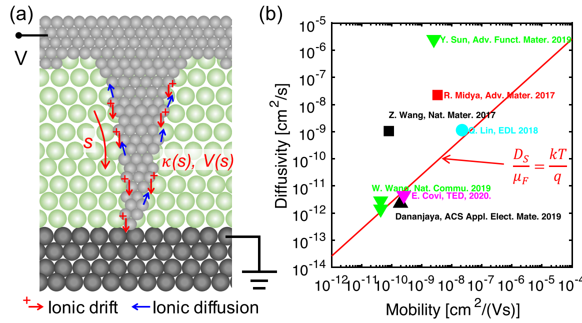

Fig. 7. (a) Schematic of the equilibrium state with the coexistence of and competition between ionic drift and diffusion along filament surface in the metallic filamentary volatile device. (b) Correlation between the diffusivity and mobility summarized in Table I. The red line indicates Einstein relation.

concentration:

$$J_{\text{diff}} = -D_{\text{S}} \frac{dc}{ds}. \tag{11}$$

Note that the surface tension-induced surface ionic diffusion described by (10) and (11) shares the same physical origin with the Gibbs–Thomson effect [37], [38], which was recently proposed for the volatility of the Ag-based RRAM device [14], [39] and was originally proposed by Lord Kelvin (William Thomson) for the vapor–liquid surface [37]. This effect dominates only in nanoscale structure with high surface/volume ratio where the gradient of surface ionic concentration is large enough to enable detectable filament shape change in reasonable measurement timescale.

The ionic drift flux is defined as the product of ionic mobility, concentration, and electric field, namely $J_{\text{drift}} = \mu_F c F$. We finally obtain total ionic transport flux as the sum of drift and diffusion components, namely

$$J_{\text{total}} = J_{\text{drift}} + J_{\text{diff}} = \mu_F c F - D_{\text{S}} \frac{dc}{ds}. \tag{12}$$

V. Einstein Relation for Ionic Transport

Similar to the electron transport in semiconductors, we can define an additional variable, namely chemical potential μ, which is the sum of surface energy and electrostatic energy

$$\mu(s) = \kappa(s)\gamma\delta^3 + qV(s) \tag{13}$$

where s denotes the coordinate along the surface the filament [Fig. 7(a)] and q is the charge of Cu/Ag ions. We expect that the metallic filament charge is overall neutral and the metallic filament can be modeled as a mixture of Cu/Ag ions and an equal number of conduction-band electrons. Under an applied electric field, electrons drift from cathode to anode, while Cu/Ag ions drift from anode to cathode. This can explain how ionic migration can take place within a neutral metallic phase. For simplicity, we always assumed the charge q to be a single positive elementary charge for both Ag and Cu. Both items on the right-hand side of (13) have the unit of energy. If we assume an ideal state where the chemical potential is a constant along the filament surface from one electrode to the other electrode, that is the equilibrium state, we can expect a naturally zero ionic flux, thus

$$d\mu(s)/ds = 0, \quad J_{\text{total}} = 0. \tag{14}$$

Substituting (12) and (13) to (14), we obtain the Einstein relation for ionic drift–diffusion transport, namely

$$D_{\text{S}}/\mu_0 = kT/q \tag{15}$$

which indicates an intimate relationship between ionic mobility and ionic diffusivity. Note the equilibrium state in (14) only holds at low electric field, thus the mobility in (15) is the low electric mobility μ_0.

Equation (15) can be validated by a comparison with reported data in the literature. In addition to our own measurement results [15], we collected the switching time data and retention from previous reports [1]–[3], [6], [7], [29], [40] as summarized in Table I. We can obtain the ionic mobility and ionic diffusivity from the switching data and retention time data, through our switching model [(3)] and retention model [(9)], respectively. The values of parameters are $\alpha = 0.09$, $\gamma = 1$ J/m^2, $\delta = 2.9$ Å, $V_c = 0.4$ V, $\sigma_0 = 5 \times 10^5$ S/m. Note that the silver conductivity is assumed much smaller than the bulk conductivity, since the filament size is very small compared to free electron path length [41]. Fuchs–Sondheimer equation [41] would be more accurate for the calculation of the size-dependent conductivity of the Ag filament. However, we decided to assume a constant conductivity, since the exact shape of the filament is not known.

Fig. 7(b) shows all the correlation plot of ionic diffusivity as a function of mobility, compared with the Einstein relation. From the data points, we see that the Einstein law of (15) generally provides an overestimation of ionic diffusivity. This can be explained by excessive oxidation–bulk transport–reduction of the Ag atoms in the initial stage of the switching process, which can be viewed as corresponding to tunneling effect in electron transport and might be incorporated in this framework of ionic transport theory.

VI. Read Voltage Dependent Retention Time

We can further check on the ionic drift and diffusion theory by an experiment where the ionic drift and diffusion coexist and are competing with each other. In the companion paper, we showed that the retention time is actually affected by the read voltage [15]. A larger read voltage would generally result in a longer retention time as shown in Fig. 8. According to our model, when the read voltage approximates the dc hold voltage V_{Hold}, an equilibrium state is established, thus

$$\kappa(s)\gamma\delta^3 + q\psi_{\text{Hold}}(s) = 0 \tag{16}$$

where the $\psi_{\text{Hold}}(s)$ denotes the electrostatic potential profile along the filament at this equilibrium state. At relatively small read voltage $V_{\text{Read}} < V_{\text{Hold}}$, the $\kappa(s)$'s contribution to the ionic chemical potential would not change, while the electrostatic contribution would scale down by a factor $V_{\text{Read}}/V_{\text{Hold}}$, namely, $\psi(s) = (V_{\text{Read}}/V_{\text{Hold}})\psi_{\text{Hold}}(s)$. By combining it

TABLE I

SUMMARY OF THE SWITCHING TIME, RETENTION TIME AND OTHER PARAMETERS OF Ag/Cu-BASED VOLATILE DEVICES FROM THE LITERATURE

Device	$t_{ox}(nm)$	$V_{T,DC}(V)$	$V_P(V)$	t_{set}	I_C	t_R	μ_0 $(cm^2/(V\cdot s))$	D_S (cm^2/s)	Ref.
Pt/SiO$_x$N$_y$:Ag/Pt	15	0.3	0.8	5 ms	1 mA	30 ms	7.97×10^{-11}	1.05×10^{-9}	[7]
Pd/Ag/HfO$_x$Ag/Pd	5	0.35	2	75 ns	40 μA	250 ns	3.34×10^{-9}	2.25×10^{-8}	[1]
Ag/defected-graphene/SiO$_2$/Pt	40	0.7	2	100 ns	450 μA	1 μs	6.83×10^{-7}	2.55×10^{-5}	[6]
TiW/CuS/GeSe/Pt	15	0.5	1.7	672 ns	60 μA	100 μs	2.19×10^{-8}	1.14×10^{-9}	[2]
Ag/TaO$_x$/TaO$_y$/TaO$_x$/Ag	50	0.1	3	75 ns	60 μA	500 ns	2.51×10^{-9}	2.52×10^{-6}	[3]
AgNW/Silk/AgNW	10	0.7	2	100 μs	100 μA	100 ms	4.27×10^{-11}	1.40×10^{-12}	[29]
					1 mA	10 s		2.81×10^{-12}	
Pt/HfO$_x$/Cu/Pt	10	0.21	1	210 μs	21 μA	2.7 ms	1.96×10^{-10}	2.29×10^{-12}	[40]
Ag/SiO$_x$/C	5	1.9	2–2.5	0.1–10 ms	9–70 μA	1 μs–1 s	2.5×10^{-10}	4.44×10^{-12}	[15]

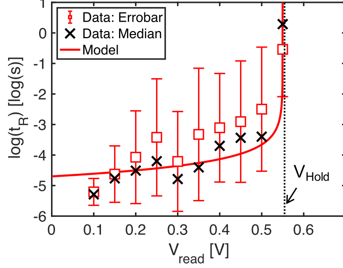

Fig. 8. Experimental retention time as a function of read voltage fitted with the calculation line, confirming competition between ionic drift and diffusion.

with (16), we can get the chemical potential profile at the specific read voltage

$$\mu_{\text{Read}}(s) = \frac{V_{\text{Hold}} - V_{\text{Read}}}{V_{\text{Hold}}} q\,\psi_{\text{Hold}}(s). \tag{17}$$

Then the retention time can be obtained by the integration of time elapsed for the filament break at the read voltage reduced total ionic flux rate

$$t_R = \int dt \propto \frac{1}{\nabla_s \cdot J_{\text{total}}} \propto \frac{1}{\nabla_s \cdot \frac{d\mu(s)}{ds}} \propto \frac{V_{\text{Hold}}}{V_{\text{Hold}} - V_{\text{Read}}} \tag{18}$$

which suggests that retention time increases with the increase of read voltage in agreement with experimental data [15]. Also, (18) predicts an infinite retention time for the read voltage approaching the hold voltage. We can rewrite (18) as

$$t_R = t_{R0}\frac{V_{\text{Hold}}}{V_{\text{Hold}} - V_{\text{Read}}} \tag{19}$$

where t_{R0} is the retention time at zero read voltage.

Fig. 8 shows the retention time as a function of the read voltage compared to calculations by (19). This suggests that the ionic drift and diffusion flux are competing with each other when a voltage is applied during the retention process. These results suggest that the retention time can be suitably controlled by the read condition, which might be useful in the design of neuromorphic circuits.

VII. DISCUSSION

A. Oxide Layers and Limitations of the Proposed Model

In our modeling scenario, we only account for the physical changes in the switching layer, that is, as an assumption we consider no chemical reactions between the metallic filament and the hosting materials. However, it does not exclude Ag oxidization/reduction playing contributing roles in the filament formation and disruption. For the devices with a solid electrolyte as the switching layer, for instance, Ag_2S [42], [43] and CuS [44] as switching layers for Ag and Cu electrodes, respectively, the Ag and Cu electrodes should be viewed as the "chemically active" materials. In these devices, chemical reactions as in the framework of electrochemical metallization (ECM) [26], [45], [46] are not negligible and might be the dominating mechanism. A hybrid approach combining the proposed theory with electrochemical theory should be used for further analysis of these devices.

A further evidence supporting the proposed purely physical model is the demonstration of the Ag-based volatile RRAM device with vacuum switching layer, which has been recently reported by Ji *et al.* [21]. The dc switching parameters and ac dynamics parameters are similar to the devices with oxide switching layers. This evidence also confirms that the oxide materials replacing the vacuum would not significantly influence the model parameters.

In our model, we assume that the hosting oxide materials can adjust their shape according to the growth or shape evolution of the Ag filament, similar to the ideal case of vacuum switching layer. With this assumption, in the retention model, different oxide materials will influence the surface energy of the silver filament, changing it from a surface energy in the vacuum (1 J/m^2) to an interfacial energy between the Ag and the oxide materials. These changes might result in a scaling factor on the diffusivity of the ion motion on silver filament surface. Since we linked the retention process to the switching process via the Einstein relation, we can project that the change in the switching model should be very similar, thus resulting only in a relatively small scaling factor of the mobility.

B. Comparisons With Previous Models

As mentioned in Section II, there have been several models [22]–[28] dealing with the switching dynamics of the nonvolatile filamentary RRAM devices. In the nonvolatile filamentary RRAM devices, the switching OFF of the devices is also stimulated by external voltage but with opposite polarity, i.e., bipolar switching. The voltage-controlled switching OFF of the device is considered as the reversed process of the switching ON process. However, these models could not explain the phenomena of spontaneous switching OFF of the

devices within a similar structure, i.e., the short-term retention reported here.

Strictly speaking, the "field-driven particle motion" should be defined as "drift," while "diffusion" should only refer to "concentration-driven particle motion" following to Fick's law. The concept of "electric field driven ion diffusion" is generally overlooked, although sometimes appears in the literature [24]. In some previous models, "ionic drift" corresponds to the *vertical* migration of ions within the oxide materials, while the "ionic diffusion" refers to the *lateral* out diffusion of atoms from the filament to surrounding materials [47], [48]. These two processes occur in different scenarios (applied voltage, direction, local temperature), thus should not be theoretically linked by the Einstein relation. For the same reason, "filament dissolution" for switching-OFF of the metallic filamentary device might be a misleading concept, which is implying that the filament atoms are out diffusing to surrounding materials, while, in several TEM observations, the filament is subject to clustering and retraction other than out diffusion [6], [7], [12], [35].

In this work, for the switching ON model, we propose the mechanism of electric field driven motion of surface atoms. The mechanism is based on several considerations: 1) Ag and Cu are not "chemically active" materials as discussed in Section VII-A; 2) in TEM observations, continuous filaments are usually observed at least for relatively large compliance currents; continuous filaments between top electrode and bottom electrode and their abrupt break are consistent with the high ON/OFF ratio in dc switching data; and 3) the electric field inside the metallic filament should be virtually zero according to Gauss's law.

For the retention model, i.e., the spontaneous switching OFF model, based on our previous studies [29], [31], [49], we proposed the mechanism of surface tension driven clustering effect. The basic idea is that the convex point has a higher surface atomic concentration compared to the trough point. We notice that surface tension is also the driving force causing liquid materials to tend to droplet formation, which for solid materials, i.e., Ag in the present case, is only effective at the nanoscale. In fact, the droplet-like clustering of Ag nanowires [50], also referred to as Rayleigh instability [30], has been previously reported. Utilizing this mechanism, we can explain multiple experimental observations in Ag and Cu nanoscale filamentary volatile RRAM devices, for instance, the compliance current/filament size dependent retention time [31], transition from volatile to nonvolatile switching behaviors [29], the generally high ON/OFF resistance ratio [49], and the ovulation effect of generating spherical particles [15], [29]. Most importantly, this mechanism provides us a quantitative method to describe the filament disruption and clustering processes. In fact, previous attempts only use a qualitative explanation based on the "nucleation energy" [27], [51], while our model relies on a physical foundation to describe the energy minimization driven process.

In this work, we link the ionic drift and diffusion processes by the Einstein relation. The validity of Einstein relation for ionic motion is not straightforward: in fact, the field-driven particle motion and gradient-driven diffusion must occur in the same conditions. In our case, both drift and diffusion occur at the surface of a continuous filament. Previous models dealing with the Einstein relation of ionic drift–diffusion assume the bulk ionic transport [47], [52], [53], where the bulk diffusion will not result in clustering of the filaments as observed in filamentary volatile RRAM devices.

VIII. Conclusion

In summary, the switching and retention models for volatile RRAM devices are presented to quantitatively describe these two critical processes for device operating. The models can also be used for extracting internal properties (i.e., ionic mobility and diffusivity) of ionic devices. Furthermore, the switch-ON and -OFF processes of the metallic filamentary-based volatile device are explained by ionic drift–diffusion theory and are further associated with Einstein relation. Finally, we can predict that the depth insight of the switching mechanism and ionic transport theory could enhance our understanding of novel electron devices which involve atomic/ionic transport and structure reconfiguration, and the switching and retention models will also enable advanced compact models.

References

[1] R. Midya *et al.*, "Anatomy of Ag/Hafnia-based selectors with 10^{10} nonlinearity," *Adv. Mater.*, vol. 29, no. 12, Mar. 2017, Art. no. 1604457, doi: 10.1002/adma.201604457.

[2] Q. Lin *et al.*, "Dual-layer selector with excellent performance for cross-point memory applications," *IEEE Electron Device Lett.*, vol. 39, no. 4, pp. 496–499, Apr. 2018, doi: 10.1109/LED.2018.2808465.

[3] Y. Sun *et al.*, "Performance enhancing selector via symmetrical multilayer design," *Adv. Func. Mater.*, vol. 29, no. 13, Mar. 2019, Art. no. 1808376, doi: 10.1002/adfm.201808376.

[4] M. Wang *et al.*, "Enhancing the matrix addressing of flexible sensory arrays by a highly nonlinear threshold switch," *Adv. Mater.*, vol. 30, no. 33, Aug. 2018, Art. no. 1802516, doi: 10.1002/adma.201802516.

[5] Q. Luo *et al.*, "Cu BEOL compatible selector with high selectivity ($>10^7$), extremely low off-current ($\sim$pA) and high endurance ($>10^{10}$)," in *IEDM Tech. Dig.*, Dec. 2015, pp. 10.4.1–10.4.4, doi: 10.1109/IEDM.2015.7409669.

[6] X. Zhao *et al.*, "Breaking the current-retention dilemma in cation-based resistive switching devices utilizing graphene with controlled defects," *Adv. Mater.*, vol. 30, no. 14, Apr. 2018, Art. no. 1705193, doi: 10.1002/adma.201705193.

[7] Z. Wang *et al.*, "Memristors with diffusive dynamics as synaptic emulators for neuromorphic computing," *Nature Mater.*, vol. 16, no. 1, pp. 101–108, Jan. 2017, doi: 10.1038/nmat4756.

[8] W. Wang *et al.*, "Learning of spatiotemporal patterns in a spiking neural network with resistive switching synapses," *Sci. Adv.*, vol. 4, no. 9, Sep. 2018, Art. no. eaat4752, doi: 10.1126/sciadv.aat4752.

[9] Y. Zhang *et al.*, "Highly compact artificial memristive neuron with low energy consumption," *Small*, vol. 14, no. 51, Dec. 2018, Art. no. 1802188, doi: 10.1002/smll.201802188.

[10] F. G. Aga *et al.*, "Retention modeling for ultra-thin density of Cu-based conductive bridge random access memory (CBRAM)," *AIP Adv.*, vol. 6, no. 2, Feb. 2016, Art. no. 025203, doi: 10.1063/1.4941752.

[11] D. Ielmini, F. Nardi, C. Cagli, and A. L. Lacaita, "Size-dependent retention time in NiO-based resistive-switching memories," *IEEE Electron Device Lett.*, vol. 31, no. 4, pp. 353–355, Apr. 2010, doi: 10.1109/LED.2010.2040799.

[12] F. Yuan *et al.*, "Real-time observation of the electrode-size-dependent evolution dynamics of the conducting filaments in a SiO_2 layer," *ACS Nano*, vol. 11, no. 4, pp. 4097–4104, Apr. 2017, doi: 10.1021/acsnano.7b00783.

[13] H. Jiang *et al.*, "A novel true random number generator based on a stochastic diffusive memristor," *Nature Commun.*, vol. 8, no. 1, p. 882, Oct. 2017, doi: 10.1038/s41467-017-00869-x.

[14] Z. Wang *et al.*, "Fully memristive neural networks for pattern classification with unsupervised learning," *Nature Electron.*, vol. 1, no. 2, pp. 137–145, Feb. 2018, doi: 10.1038/s41928-018-0023-2.

[15] E. Covi, Y.-H. Lin, W. Wang, M. Farronato, E. Ambrosi, and D. Ielmini, "Switching dynamics of Ag based filamentary volatile resistive switching devices—Part I: Experimental characterization," *IEEE Trans. Electron Devices*, vol. 68, no. 9, pp. 4335–4341, Sep. 2021.

[16] W. Wang, E. Covi, Y.-H. Lin, E. Ambrosi, and D. Ielmini, "Modeling of switching speed and retention time in volatile resistive switching memory by ionic drift and diffusion," in *IEDM Tech. Dig.*, Dec. 2019, p. 32, doi: 10.1109/IEDM19573.2019.8993625.

[17] R. Waser, R. Dittmann, G. Staikov, and K. Szot, "Redox-based resistive switching memories–nanoionic mechanisms, prospects, and challenges," *Adv. Mater.*, vol. 21, nos. 25–26, pp. 2632–2663, Jul. 2009, doi: 10.1002/adma.200900375.

[18] Q. Liu *et al.*, "Real-time observation on dynamic growth/dissolution of conductive filaments in oxide-electrolyte-based ReRAM," *Adv. Mater.*, vol. 24, no. 14, pp. 1844–1849, Apr. 2012, doi: 10.1002/adma.201104104.

[19] C. Schindler, G. Staikov, and R. Waser, "Electrode kinetics of Cu-SiO_2-based resistive switching cells: Overcoming the voltage-time dilemma of electrochemical metallization memories," *Appl. Phys. Lett.*, vol. 94, no. 7, pp. 92–95, 2009, doi: 10.1063/1.3077310.

[20] S. Menzel, U. Böttger, M. Wimmer, and M. Salinga, "Physics of the switching kinetics in resistive memories," *Adv. Funct. Mater.*, vol. 25, no. 40, pp. 6306–6325, Oct. 2015, doi: 10.1002/adfm.201500825.

[21] X. Ji, S. Hao, K. Y. Pang, K. G. Lim, and R. Zhao, "A vacuum gap selector with ultra-low leakage for large-scale neuromorphic network," *IEEE Electron Device Lett.*, vol. 41, no. 3, pp. 505–508, Mar. 2020, doi: 10.1109/LED.2020.2969438.

[22] J. R. Jameson *et al.*, "One-dimensional model of the programming kinetics of conductive-bridge memory cells," *Appl. Phys. Lett.*, vol. 99, no. 6, Aug. 2011, Art. no. 063506, doi: 10.1063/1.3623485.

[23] S. Yu and H.-S.-P. Wong, "Compact modeling of conducting-bridge random-access memory (CBRAM)," *IEEE Trans. Electron Devices*, vol. 58, no. 5, pp. 1352–1360, May 2011, doi: 10.1109/TED.2011.2116120.

[24] A. Nayak *et al.*, "Rate-limiting processes determining the switching time in a Ag_2S atomic switch," *J. Phys. Chem. Lett.*, vol. 1, no. 3, pp. 604–608, Feb. 2010, doi: 10.1021/jz900375a.

[25] A. Nayak, T. Tsuruoka, K. Terabe, T. Hasegawa, and M. Aono, "Switching kinetics of a Cu_2S-based gap-type atomic switch," *Nanotechnology*, vol. 22, no. 23, Jun. 2011, Art. no. 235201, doi: 10.1088/0957-4484/22/23/235201.

[26] S. Menzel, S. Tappertzhofen, R. Waser, and I. Valov, "Switching kinetics of electrochemical metallization memory cells," *Phys. Chem. Chem. Phys.*, vol. 15, no. 18, p. 6945, 2013, doi: 10.1039/c3cp50738f.

[27] M. Lübben, S. Menzel, S. G. Park, M. Yang, R. Waser, and I. Valov, "SET kinetics of electrochemical metallization cells: Influence of counter-electrodes in SiO_2/Ag based systems," *Nanotechnology*, vol. 28, no. 13, Mar. 2017, Art. no. 135205, doi: 10.1088/1361-6528/aa5e59.

[28] P. Bousoulas *et al.*, "Investigating the origins of ultra-short relaxation times of silver filaments in forming-free SiO_2-based conductive bridge memristors," *Nanotechnology*, vol. 31, no. 45, Nov. 2020, Art. no. 454002, doi: 10.1088/1361-6528/aba3a1.

[29] W. Wang *et al.*, "Surface diffusion-limited lifetime of silver and copper nanofilaments in resistive switching devices," *Nature Commun.*, vol. 10, no. 1, p. 81, Jan. 2019, doi: 10.1038/s41467-018-07979-0.

[30] C.-P. Hsiung *et al.*, "Formation and instability of silver nanofilament in ag-based programmable metallization cells," *ACS Nano*, vol. 4, no. 9, pp. 5414–5420, Sep. 2010, doi: 10.1021/nn1010667.

[31] W. Wang *et al.*, "Volatile resistive switching memory based on ag ion drift/diffusion—Part I: Numerical modeling," *IEEE Trans. Electron Devices*, vol. 66, no. 9, pp. 3795–3801, Sep. 2019, doi: 10.1109/TED.2019.2928890.

[32] C. Herring, "Effect of change of scale on sintering phenomena," *J. Appl. Phys.*, vol. 21, no. 4, pp. 301–303, Apr. 1950, doi: 10.1063/1.1699658.

[33] D. Ielmini, "Modeling the universal set/reset characteristics of bipolar RRAM by field- and temperature-driven filament growth," *IEEE Trans. Electron Devices*, vol. 58, no. 12, pp. 4309–4317, Dec. 2011, doi: 10.1109/TED.2011.2167513.

[34] B.-G. Chae *et al.*, "Nanometer-scale phase transformation determines threshold and memory switching mechanism," *Adv. Mater.*, vol. 29, no. 30, Aug. 2017, Art. no. 1701752, doi: 10.1002/adma.201701752.

[35] Y. Yang *et al.*, "Electrochemical dynamics of nanoscale metallic inclusions in dielectrics," *Nature Commun.*, vol. 5, no. 1, p. 4232, Sep. 2014, doi: 10.1038/ncomms5232.

[36] G. C. Kuczynski, "Self-diffusion in sintering of metallic particles," *JOM*, vol. 1, no. 2, pp. 169–178, Feb. 1949, doi: 10.1007/BF03398090.

[37] W. Thomson, "LX. On the equilibrium of vapour at a curved surface of liquid," *London, Edinburgh, Dublin Phil. Mag. J. Sci.*, vol. 42, no. 282, pp. 448–452, Dec. 1871, doi: 10.1080/14786447108640606.

[38] W. W. Mullins, "Theory of thermal grooving," *J. Appl. Phys.*, vol. 28, no. 3, pp. 333–339, Mar. 1957, doi: 10.1063/1.1722742.

[39] S. Savel'ev, F. Marchesoni, and F. Nori, "Stochastic transport of interacting particles in periodically driven ratchets," *Phys. Rev. E, Stat. Phys. Plasmas Fluids Relat. Interdiscip. Top.*, vol. 70, no. 6, Dec. 2004, Art. no. 061107, doi: 10.1103/PhysRevE.70.061107.

[40] P. A. Dananjaya, D. J. J. Loy, S. C. W. Chow, and W. S. Lew, "Unidirectional threshold switching induced by Cu migration with high selectivity and ultralow off current under gradual electroforming treatment," *ACS Appl. Electron. Mater.*, vol. 1, no. 10, pp. 2076–2085, Oct. 2019, doi: 10.1021/acsaelm.9b00446.

[41] D. Gall, "Electron mean free path in elemental metals," *J. Appl. Phys.*, vol. 119, no. 8, Feb. 2016, Art. no. 085101, doi: 10.1063/1.4942216.

[42] K. Terabe, T. Hasegawa, T. Nakayama, and M. Aono, "Quantized conductance atomic switch," *Nature*, vol. 433, no. 7021, pp. 47–50, Nov. 2005, doi: 10.1038/nature03202.1.

[43] T. Ohno, T. Hasegawa, T. Tsuruoka, K. Terabe, J. K. Gimzewski, and M. Aono, "Short-term plasticity and long-term potentiation mimicked in single inorganic synapses," *Nature Mater.*, vol. 10, no. 8, pp. 591–595, Aug. 2011, doi: 10.1038/nmat3054.

[44] T. Sakamoto, H. Sunamura, H. Kawaura, T. Hasegawa, T. Nakayama, and M. Aono, "Nanometer-scale switches using copper sulfide," *Appl. Phys. Lett.*, vol. 82, no. 18, pp. 3032–3034, May 2003, doi: 10.1063/1.1572964.

[45] R. Waser and M. Aono, "Nanoionics-based resistive switching memories," *Nature Mater.*, vol. 6, no. 11, pp. 833–840, Nov. 2007, doi: 10.1038/nmat2023.

[46] I. Valov, R. Waser, J. R. Jameson, and M. N. Kozicki, "Electrochemical metallization memories—Fundamentals, applications, prospects," *Nanotechnology*, vol. 22, no. 28, Jul. 2011, Art. no. 289502, doi: 10.1088/0957-4484/22/28/289502.

[47] D. B. Strukov and R. S. Williams, "Exponential ionic drift: Fast switching and low volatility of thin-film memristors," *Appl. Phys. A, Solids Surf.*, vol. 94, no. 3, pp. 515–519, Mar. 2009, doi: 10.1007/s00339-008-4975-3.

[48] X. Zhao *et al.*, "Confining cation injection to enhance CBRAM performance by nanopore graphene layer," *Small*, vol. 13, no. 35, Sep. 2017, Art. no. 1603948, doi: 10.1002/smll.201603948.

[49] W. Wang *et al.*, "Volatile resistive switching memory based on ag ion drift/diffusion—Part II: Compact modeling," *IEEE Trans. Electron Devices*, vol. 66, no. 9, pp. 3802–3808, Sep. 2019, doi: 10.1109/TED.2019.2928888.

[50] J. Sun *et al.*, "Liquid-like pseudoelasticity of sub-10-nm crystalline silver particles," *Nature Mater.*, vol. 13, no. 11, pp. 1007–1012, Nov. 2014, doi: 10.1038/nmat4105.

[51] I. Valov *et al.*, "Atomically controlled electrochemical nucleation at superionic solid electrolyte surfaces," *Nature Mater.*, vol. 11, no. 6, pp. 530–535, Jun. 2012, doi: 10.1038/nmat3307.

[52] R. Meyer, R. Liedtke, and R. Waser, "Oxygen vacancy migration and time-dependent leakage current behavior of $Ba_{0.3}Sr_{0.7}TiO_3$ thin films," *Appl. Phys. Lett.*, vol. 86, no. 11, Mar. 2005, Art. no. 112904, doi: 10.1063/1.1874313.

[53] S. Larentis, F. Nardi, S. Balatti, D. C. Gilmer, and D. Ielmini, "Resistive switching by voltage-driven ion migration in bipolar RRAM—Part II: Modeling," *IEEE Trans. Electron Devices*, vol. 59, no. 9, pp. 2468–2475, Sep. 2012, doi: 10.1109/TED.2012.2202320.